Hindawi
Structural Control and Health Monitoring
Volume 2024, Article ID 8817461, 17 pages
https://doi.org/10.1155/2024/8817461

WILEY | Hindawi

Research Article

The Parameter Identification of Structure with TMD considering Seismic Soil-Structure Interaction

Shutong Liu,[1] **Haochen Li**,[1] **Song Tang**,[1] **Jinlun Xie**,[2] **Shutong Yang**,[1] **and Peizhen Li**[2]

[1]*College of Engineering, Ocean University of China, Qingdao 266100, China*
[2]*State Key Laboratory of Disaster Reduction in Civil Engineering, Tongji University, Shanghai 200092, China*

Correspondence should be addressed to Peizhen Li; lipeizh@tongji.edu.cn

Received 25 August 2023; Revised 28 February 2024; Accepted 30 March 2024; Published 23 April 2024

Academic Editor: Tzu-Kang Lin

Parameter identification is of great significance for the postearthquake performance evaluation of structure equipped with tuned mass damper (TMD). However, the soil-structure interaction (SSI) effects have not been considered in the parameter identification of structure with TMD yet, which influence the dynamic characteristics and seismic responses of structures. This paper aims at proposing a framework for identifying the physical parameters of soil-structure-TMD system. Firstly, the accelerated particle swarm optimization (APSO) algorithm is combined with the search space reduction (SSR) method. Then, the frequency response function and transmissibility function are adopted for output-input and input-only cases, respectively, and a simplified mechanical model for soil-structure-TMD system is employed. Next, the measured responses are used to identify the physical parameters of structure with TMD considering SSI effects. Finally, the effectiveness of the proposed identification method is investigated, and the influences of frequency band and noise pollution on the identification performance are discussed. The results show that the proposed strategy can identify the system physical parameters accurately and quickly. It is worth noting that high frequency bands and noise pollution may lead to estimation error, especially for output-only case.

1. Introduction

Structural control technologies are commonly adopted to mitigate the induced vibrations of structures caused by earthquake, and many novel devices for structural vibration control have been developed in the last few decades [1–5]. The tuned mass damper (TMD) consisting of mass, stiffness, and damping components is one of the most promising and effective devices, and its vibration control performance has been widely investigated [6]. However, the variation in primary structure and TMD properties would greatly influence TMD's performance on the suppression of structural vibration [7–9].

Parameter identification is crucial to estimate the dynamic characteristics of a structural system through ambient vibration measurements, which can serve as a basis for condition assessment, structural damage detection, and long-term health monitoring. Many advanced methods have been utilized for the parameter estimation of civil engineering structures [10–14]. Love et al. [15] estimated the inherent structural damping of structure-TMD system using the random decrement technique. Weber et al. [16] assessed the long-term performance of pedestrian bridge with TMDs by identifying system parameters. Wang et al. [17] utilized a Bayesian method to obtain the modal parameters of the primary structure with TMD. Yuan et al. [18] integrated the second-order blind identification method with the empirical wavelet transform to get the modal frequencies and damping of structure with TMD. Cao et al. [19] used the stochastic subspace technique to identify the modal properties of the coupled structure-TMD system. Cho et al. [20] derived decoupled equations of motion for identifying dynamic properties of secondary mass dampers by the full-scale field test. The methods proposed in the above studies for identifying the parameters of the structure-TMD system have good identification accuracy in specific cases. However, the iterative process of most methods is complicated, and some methods show low accuracy in identifying parameters at high frequency range. Roffel et al. [21] obtained

the modal properties of structures with a pendulum TMD using the Extended Kalman Filter. Schleiter et al. [22] employed an adaptive unscented Kalman filter scheme to identify the system parameters for variable stiffness TMDs. Hwang et al. [23] extracted modes using a modal-based Kalman filter for damped structures. As one of the most commonly used identification methods, the filtering methods are computationally intensive and not suitable for perform multi-degree-of-freedom identification.

The soil-structure interaction (SSI) influences the dynamic characteristics of the structure [24], such as period and damping, and seismic responses of the structure [25]. In the soil-structure-TMD system, the seismic response of the structure is affected by soil, TMD, and their coupling effects. Consequently, it is important to consider the SSI effects on structure equipped with TMD, especially on flexible soil. Liu et al. [26, 27] and Jabary et al. [28, 29] conducted shaking table tests and geotechnical centrifuge tests to explore the effectiveness of TMD for multi-story frames considering SSI effects, respectively. Jia et al. [30] discussed the influence of a variety of parameters on TMD performance including SSI effects by a fully 3D model. Abd-Elhamed et al. [31] compared the seismic response of TMD controlled building with that of uncontrolled case. Gorini et al. [32] established a general nondimensional formulation for the linear soil-structure-TMD system. Khoshnoudian et al. [33] analyzed the differences of seismic responses of building structures under three foundation conditions. Zhang et al. [34] carried out a nonlinear seismic fragility assessment of a benchmark structure with TMD in the SSI system. Espinoza et al. [35] studied the torsional control performance of TMD involving seismic soil-structure interaction. Bekdaş et al. [36] and Djedoui et al. [37] adopted metaheuristic algorithms for the optimization of TMD parameters considering SSI effects. Gao et al. [38] simulated the SSI system employing lumped parameter models to investigate the TMD performance. From the above studies, it can be concluded that SSI effects may become crucial in the seismic response of structure and the seismic control performance of TMD, so including SSI effects would reflect the work condition of structure and TMD under earthquake excitations more actually.

Nevertheless, the previous studies on parameter identification of structure equipped with TMD have not taken soil-structure interaction into consideration, and the parameter identification of structure equipped with TMD in the presence of seismic SSI is rarely reported. Hence, this paper conducted the parameter identification of soil-structure-TMD system. The accelerated particle swarm optimization (APSO) algorithm combined with the search space reduction (SSR) method is proposed for the parameter estimation of soil-structure-TMD system. Furthermore, the frequency response function and transmissibility function are used for output-input and output-only cases, respectively. The rationality of the identification method is verified by numerical simulation, and some factors on identification accuracy are considered. This study is of great practical significance to develop a parameter identification framework of structure with TMD including SSI effects.

The rest of this paper mainly consists of the following. Section 2 introduces the identification methodology in detail. Section 3 describes a brief overview of the numerical model for this study. The identification results are elaborated and discussed in Sections 4 and 5. Section 6 summarizes the conclusions.

2. Methodology

2.1. Transmissibility Function. The motion equation of structure with N degrees of freedom (DOFs) can be expressed as

$$[M]\{\ddot{x}(t)\} + [C]\{\dot{x}(t)\} + [K]\{x(t)\} = \{f(t)\}, \tag{1}$$

where $[M]$, $[C]$, and $[K]$ are the mass, damping, and stiffness matrices, respectively, and $f(t)$ is the external force. By Fourier transform, the frequency response function $H(\omega)$ can be obtained through the ratio of the measured forces $F(\omega)$ and vibration responses $X(\omega)$.

$$H(\omega) = \frac{\{X(\omega)\}}{\{F(\omega)\}}. \tag{2}$$

Assuming that $x_i(t)$ and $x_o(t)$ are the response records of measuring points i and o, the transmissibilities are defined as the ratio of the two response spectra [39], namely:

$$T_{io}(\omega) = \frac{X_i(\omega)}{X_o(\omega)}, \tag{3}$$

where $X_i(\omega)$ and $X_o(\omega)$ are response spectra of $x_i(t)$ and $x_o(t)$, respectively. When multiple excitations are applied on the system, the transmissibility can be expressed as [40]

$$T_{io}(\omega) = \frac{X_i(\omega)}{X_o(\omega)} = \frac{\sum_{m=1}^{N_F} H_{i,m}(\omega) F_m(\omega)}{\sum_{m=1}^{N_F} H_{o,m}(\omega) F_m(\omega)}, \tag{4}$$

where $H_{i,m}(\omega)$ is the frequency response function corresponding to the input-output transitive relation of the i and m DOFs; $F_m(\omega)$ represents the Fourier transform coefficients of external excitation at m DOF; and N_F is the number of measured points. In this paper, the frequency response function and transmissibility function are used for identifying structural physical parameters for a priori known seismic input (output-input) and a priori unknown seismic input (output-only) situations, respectively.

2.2. APSO-SSR. The accelerated particle swarm optimization (APSO) algorithm is an improved version of PSO algorithm that avoids the problem of premature convergence, and it has the advantages of concise concept, convenient implementation, and fast convergence speed [41, 42]. The main steps of APSO algorithm are as follows [43]:

Step 1. Initialize the particle swarm. Set the maximum evolution algebra $T_{\max}$ and the population size n. In this study, the population size n and iteration times $T_{\max}$ are taken as 100 and 50, respectively. Randomly generate n particle groups $X_1, X_2, \ldots, X_n$ in the defined space R^n to form the initial population $X(t)$ $(t = 1)$ and initial velocities $V_1, V_2, \ldots, V_n$ for each particle.

Step 2. Evaluate particle swarm $X(t)$. Calculate the fitness value of each particle in the population and compare the current fitness value of the particle with $p_{\text{best}i}$. If it is better, set its position as the current optimal position of particle i in the D-dimensional space.

Step 3. For each particle, compare its current fitness value with the global optimal solution g_{best} of the population. If it is better, update its position to the current global best position of the population. Update the velocity and position of particles to generate a new population $X_{(t+1)}$.

Step 4. Check if the end condition is met. If it is, end the algorithm and output g_{best}; otherwise, $t = t + 1$, go to step 2. The ending condition is generally that the maximum evolutionary algebra $T_{\max}$ or the improvement degree of g_{best} less than the given accuracy ε is achieved through iterative optimization.

The search space reduction (SSR) method can improve the efficiency and accuracy of identification algorithms by reducing large parameter search space [44, 45]. Thus, this study adopts SSR method within the APSO algorithm. A number of APSO independent runs with the same original search space are parallelly conducted to evaluate the values of the objective function and the solutions. A set of solutions is obtained, and the solution with the worst fitness value is removed. The remaining $\text{PR}^{(r)}$ solutions are marked as Φ.

$$\Phi = \left\{\widehat{\psi}_k \mid k = 1, 2, \ldots, \text{PR}^{(r)}\right\}. \tag{5}$$

The weighting coefficient of each solution is expressed as

$$\omega_k = \frac{\min\left\{\text{fit}\left(\widehat{\psi}_k\right)\right\}_{k=1,2,\ldots,\text{PR}^{(r)}}}{\text{fit}\left(\widehat{\psi}_k\right)}, \tag{6}$$

where $\text{fit}(\cdot)$ is the fitness value to measure identification performance. The better identified solution has higher weights. The weighted mean value and weighted standard deviation of the i^{th} identified parameter are computed so as to determine the new parameter bounds.

$$\overline{\psi}_i = \frac{\left(\sum_{k=1}^{\text{PR}^{(r)}} \omega_k \widehat{\psi}_{ki}\right)}{\left(\sum_{k=1}^{\text{PR}^{(r)}} \omega_k\right)}, \tag{7}$$

$$\sigma_i = \sqrt{\frac{\left(\sum_{k=1}^{\text{PR}^{(r)}} \omega_k \left(\widehat{\psi}_{ki} - \overline{\psi}_i\right)^2\right)}{\left(\sum_{k=1}^{\text{PR}^{(r)}} \omega_k\right)}}. \tag{8}$$

Subsequently, the lower and upper limits of the new search space of the i^{th} identified parameter are generated:

$$\begin{aligned} \widetilde{\psi}_i^{\min} &= \overline{\psi}_i - \eta\sigma_i, \\ \widetilde{\psi}_i^{\max} &= \overline{\psi}_i + \eta\sigma_i, \end{aligned} \tag{9}$$

where η denotes the window width coefficient of the new search space, which is 5 in this study. In addition, to avoid that the new search space sometimes exceeds the original boundary, the final new space is generated by means of the intersection of the original search space and the new trial search space.

$$\left[\widehat{\psi}_i^{\min}, \widehat{\psi}_i^{\max}\right]^{\text{new}} = \left[\psi_i^{\min}, \psi_i^{\max}\right]^{\text{original}} \cap \left[\widetilde{\psi}_i^{\min}, \widetilde{\psi}_i^{\max}\right]^{\text{trial}}. \tag{10}$$

In the final new space, the APSO would conduct a new round of parameter identification and update the optimal parameter solution. The parameter identification flowchart is displayed in Figure 1.

3. Model Introduction

3.1. Mechanical Model. An N-story superstructure with TMD attached to the top floor considering SSI effects is shown in Figure 2. The dynamical SSI is complex, and thus the simplified swaying-rocking substructure model is commonly used in the parameter identification of the SSI model [46, 47]. The DOFs of primary structure, TMD, and translation-rotation foundation are N, 1, and 2, respectively, so the simplified mechanical model of soil-structure-TMD system has a total of $N + 3$ DOFs.

The motion equation of the N-story primary structure equipped with TMD on the top considering SSI effects can be written as follows:

$$[M]\ddot{x}(t) + [C]\dot{x}(t) + [K]x(t) = -[m^*]\ddot{x}_g, \tag{11}$$

where $[M]$, $[C]$, $[K]$, and $[m^*]$ represent the mass matrix, damping matrix, stiffness matrix, and acceleration mass matrix, respectively, and vectors $\ddot{x}(t)$, $\dot{x}(t)$, $x(t)$, and $\ddot{x}_g$ are the acceleration, velocity, displacement, and seismic wave acceleration vectors, respectively; see equations (12)–(20) for details. In (12)–(20), subscripts i ($i = 1, \ldots, N$), 0, and d are related to i^{th} story, foundation, and TMD, respectively.

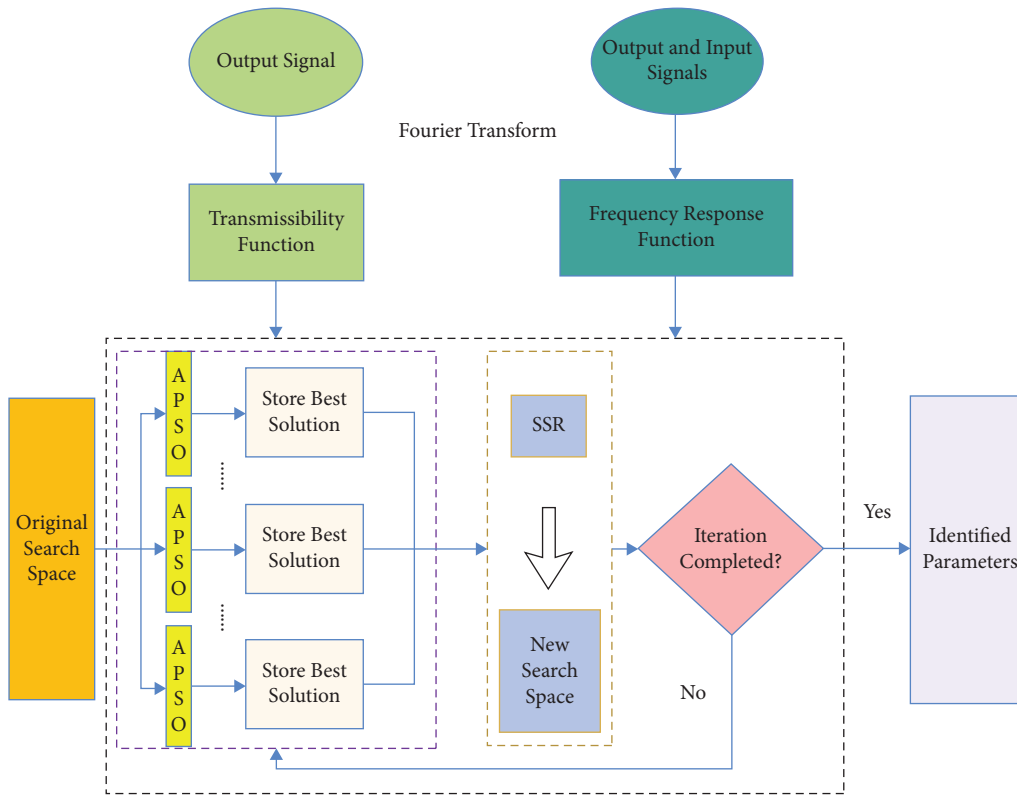

Figure 1: The parameter identification flowchart.

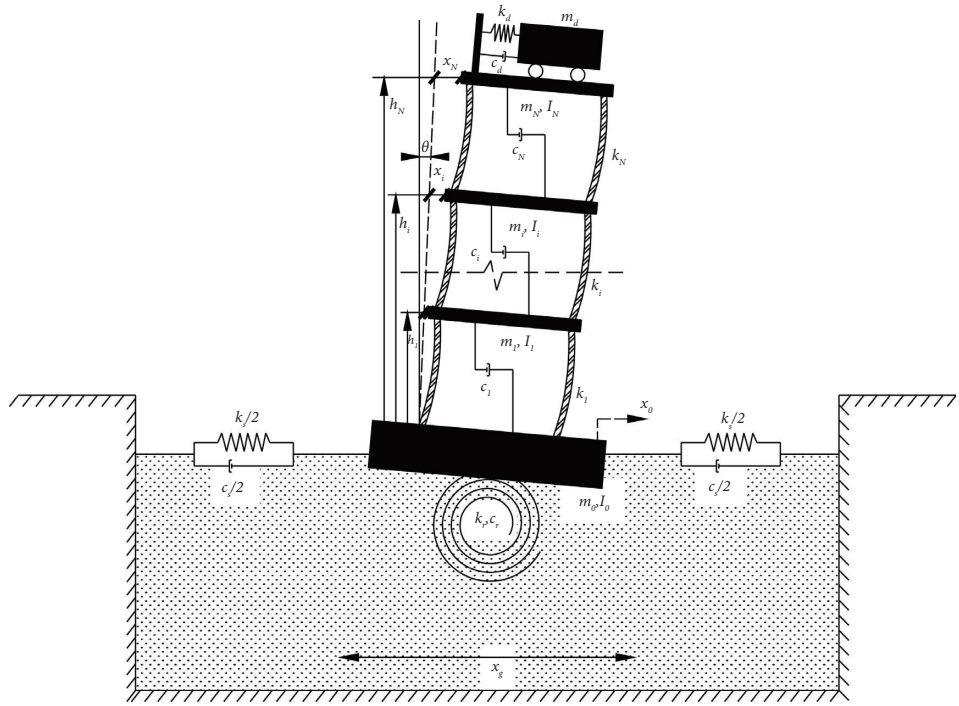

Figure 2: The mechanical model of the soil-structure-TMD system.

$$[M]=\begin{pmatrix}[M_f] & [M_v] & [MZ]\\ [M_v]^T & m_0+\left(\sum_{i=1}^{N}m_i\right)+m_d & \left(\sum_{i=1}^{N}m_ih_i\right)+m_dh_N\\ [MZ]^T & \left(\sum_{i=1}^{N}m_ih_i\right)+m_dh_N & \left(\sum_{i=1}^{N}m_ih_i^{\,2}\right)+m_dh_N^2+I_0+\sum_{i=1}^{N}I_i\end{pmatrix}, \tag{12}$$

$$[M_v]=\left[m_1,m_2,\cdots,m_{(N-1)},m_N,m_d\right]^T, \tag{13}$$

$$[MZ]=\left[m_1h_1,m_2h_2,\cdots,m_{N-1}h_{N-1},m_Nh_N,m_dh_N\right]^T, \tag{14}$$

$$[C]=\begin{pmatrix}[C_f] & 0 & 0\\ 0\cdots0 & c_s & 0\\ 0\cdots0 & 0 & c_r\end{pmatrix}, \tag{15}$$

$$[C_f]=\begin{pmatrix}(c_1+c_2) & -c_2 & & & & \\ -c_2 & (c_2+c_3) & -c_3 & & & \\ & & \ddots & & & \\ & & & -c_N & (c_N+c_d) & -c_d\\ & & & 0 & -c_d & c_d\end{pmatrix}, \tag{16}$$

$$[K]=\begin{pmatrix}[K_f] & 0 & 0\\ 0\cdots0 & k_s & 0\\ 0\cdots0 & 0 & k_r\end{pmatrix}, \tag{17}$$

$$[K_f]=\begin{pmatrix}(k_1+k_2) & -k_2 & & & & \\ -k_2 & (k_2+k_3) & -k_3 & & & \\ & & \ddots & & & \\ & & & -k_N & (k_N+k_d) & -k_d\\ & & & 0 & -k_d & k_d\end{pmatrix}, \tag{18}$$

$$[m^*]=\begin{pmatrix}m_1\\ m_2\\ \vdots\\ m_N\\ m_d\\ m_0+\sum_{i=1}^{N}m_i+m_d\\ \sum_{i=1}^{N}m_ih_i+m_dh_N\end{pmatrix}, \tag{19}$$

$$x(t)=\left[x_1,x_2,\cdots,x_{(N-1)},x_N,x_d,x_0,\theta_0\right]^T. \tag{20}$$

A five-story structure is taken as an example [48]. The story mass m_1 and foundation mass m_0 are taken as 3×10^5 kg. The story stiffness from the 1st to 5th story is $7k$, $5k$, $3k$, $2k$, and k ($k=5\times10^7$ N/m), respectively. The story mass moment of inertia I_i and foundation mass moment of inertia I_0 are 7.5×10^6 kg·m^2. The stiffness damping coefficient is taken as 0.02 without considering mass damping. The mass ratio, frequency, and damping ratio of TMD are defined as follows:

$$\mu = \frac{m_T}{M},$$
$$f_T = \frac{1}{2\pi}\omega_T = \frac{1}{2\pi}\sqrt{\frac{k_T}{m_T}}, \tag{21}$$
$$\xi = \frac{c_T}{2m_T\omega_T},$$

where μ, f_T, and ξ are the mass ratio, frequency, and damping ratio of TMD, respectively; m_T, k_T, c_T, and ω_T are the mass, stiffness, damping, and circular frequency of TMD, respectively; and M is the mass of structure.

If the TMD mass ratio μ and structural damping ratio β are known, the optimal frequency ratio and damping ratio of TMD can be expressed as follows [49]:

$$\alpha_{\text{opt}} = \frac{f_T}{f_s} = \frac{1}{1+\mu}\left[1 - \beta\sqrt{\frac{\mu}{1+\mu}}\right],$$
$$\xi_{\text{opt}} = \frac{\beta}{1+\mu} + \sqrt{\frac{\mu}{1+\mu}}, \tag{22}$$

where α_{opt} and ξ_{opt} represent the optimal frequency ratio and optimal damping ratio, respectively, and f_T and f_s are the frequencies of TMD and the primary structure, respectively. In this study, the mass ratio, frequency, and damping ratio of TMD are taken as 0.02, 0.678 Hz, and 21.53%, respectively.

The SSI effects under soft soil condition are more significant than other soil types [50]. Therefore, soft soil is taken in the structural model. The formulas for the stiffness and damping of foundation are as follows [51]:

$$V_s = \sqrt{\frac{G_s}{\rho_s}},$$
$$k_s = \frac{8G_sR_0}{2-\nu_s},$$
$$k_r = \frac{8G_sR_0^3}{3(1-\nu_s)}, \tag{23}$$
$$c_s = \frac{4.6}{2-\nu_s}\rho_sV_sR_0^2,$$
$$c_r = \frac{0.4}{1-\nu_s}\rho_sV_sR_0^4,$$

where k and c represent stiffness and damping, respectively; subscripts r and s represent translation and rotation, respectively; ν_s, V_s, G_s, and ρ_s are Poisson's ratio, shear wave velocity, shear modulus, and density of soil, respectively; and R_0 is the base radius of foundation. The specific values of the foundation parameters are shown in Table 1.

As one of the most commonly used methods for simulating nonlinear SSI effects, the equivalent linear methods have been proven to be practical and feasible by many studies [52–56]. The identification method in this study is also applicable for the equivalent linear model.

3.2. Nonstationary Earthquake Motion. The evolutionary power spectrum model of nonstationary earthquake acceleration process is adopted, and its bilateral evolutionary power spectral density function is as follows:

$$S_{U_g}(t,\omega) = A^2(t)\cdot\frac{\omega_g^4(t) + 4\xi_g^2(t)\omega_g^2(t)\omega^2}{\left[\omega^2 - \omega_g^2(t)\right]^2 + 4\xi_g^2(t)\omega_g^2(t)\omega^2} \cdot\frac{\omega^4}{\left[\omega^2 - \omega_f^2(t)\right]^2 + 4\xi_f^2(t)\omega_f^2(t)\omega^2}\cdot S_0(t), \tag{24}$$

where $S_{U_g}(t,\omega)$ is the bilateral evolution power spectral density function of the nonstationary earthquake acceleration process and $A(t)$ is the intensity modulation function.

$$A(t) = \left[\frac{t}{c}\exp\left(1 - \frac{t}{c}\right)\right]^d, \tag{25}$$

$$\omega_g(t) = \omega_0 - a\frac{l}{T},$$
$$\xi_R(t) = \xi_0 + b\frac{l}{T}, \tag{26}$$

$$\omega_f(t) = 0.1\omega_g(t),$$
$$\xi_f(t) = \xi_g(t), \tag{27}$$

where c and d are the time when the peak acceleration of seismic motion occurs and the index of the control shape, respectively; T represents the total duration of the nonstationary earthquake acceleration process; and ω_0, ξ_0, a, b, c, and d can be determined from the site classifications and design earthquake effects specified in current seismic code.

The spectral parameters $S_0(t)$ reflecting the intensity of seismic motion can be determined as

$$S_0(t) = \frac{\overline{a}_{\max^2}}{\gamma^2\left[\pi\omega_g(t)\left(2\xi_g(t) + 1/2\xi_g(t)\right)\right]}, \tag{28}$$

where $\overline{a}_{\max}$ is the mean value of the peak acceleration of random seismic motion and γ is the peak factor. The parameter values of the evolutionary power spectrum model are listed in Table 2.

3.3. Optimization Objective. The residual error is introduced to evaluate the frequency response function and transmissibility function between measurements and simulations. The objective function $J(z)$ is built:

$$J(z) = \text{erf}(\widehat{X}(\theta), X), \tag{29}$$

where erf represents the error function; $\widehat{X}(\theta)$ is the frequency response function of identified model under known excitation condition, or its transmissibility function for excitation unknown case; X is the value of the frequency response function or transmissibility function obtained from the actual measurements; and θ represents the physical parameters of the predicted model. The objective function is

Table 1: Foundation parameters.

Translational stiffness k_s (N/m)	Rotational stiffness k_r (N·m)	Translational damping c_s (N·s/m)	Rotational damping c_r (N·s·m)
9.54×10^8	9.41×10^{10}	5.48×10^7	1.41×10^9

Table 2: Parameters of the evolutionary power spectrum model.

ω_0 (s^{-1})	ξ_0	γ	a (s^{-1})	b	c (s)	T (s)
16	0.6	2.85	5	0.35	6	200

to minimize the frequency response function and transmissibility function between the measured structural response and the simulated response of the identified mathematical model.

4. Identification Results

To verify the effectiveness of the identification method based on transmissibility functions under unknown excitation condition, this paper compares it with the identification method based on frequency response function under known excitation condition. The transmissibility function and frequency response function combined with APSO-SSR are used to identify the physical parameters of a five-story structure with TMD considering SSI effects. The mass matrix is known. The lower and upper bounds of the original search space are set to

$$\begin{aligned}\mathrm{Lb} &= \left[0.01, 0.1k_1, 0.1k_2, 0.1k_3, 0.1k_4, 0.1k_5, 0.1k_s, 0.1k_r, 0.1c_s, 0.1c_r, 0.1f_T, 0.01\right],\\ \mathrm{Ub} &= \left[0.05, 1.5k_1, 1.5k_2, 1.5k_3, 1.5k_4, 1.5k_5, 1.5k_s, 1.5k_r, 1.5c_s, 1.5c_r, 1.5f_T, 0.3\right].\end{aligned} \tag{30}$$

The physical parameter identification results of soil-structure-TMD system are shown in Table 3. The results show that there is no deviation between the identified and actual values of each parameter for output-input and output-only cases. This demonstrates that the APSO-SSR method has excellent applicability and effectiveness in the two situations. Next, the differences between the two cases (output-input and output-only) in terms of frequency response function and transmissibility function are studied.

The frequency response function and transmissibility function of simulated and identified values are compared in Figures 3 and 4. In these figures, H and T represent the frequency response function and transmissibility function, respectively; corner markers 1, 2, 3, 4, 5, 6, 7, and 8 represent TMD, 1st story, 2nd story, 3rd story, 4th story, 5th story, and the translation and rotation of foundation, respectively; the first and second corners are the excitation reference point and the response reference point in the frequency response function, respectively, while both corner markers are response reference points in the transmissibility function. In general, the identified parameters based on frequency response function or transmissibility function are well matched with the numerical simulation values. This observation implies that the identification methods are successful in obtaining the physical parameters of the soil-structure-TMD system. In this sense, under unknown excitation condition, the parameter identification method based on transmissibility function is feasible and can accurately identify the actual system parameters.

5. Analysis

5.1. Frequency Band. The impacts of frequency band on the identification accuracy are further considered in this subsection, and the identification performance for output-only case at different frequency bands is analyzed through comparison with output-input case. The first five frequencies of structure with TMD considering SSI effects are 0.85 Hz, 1.16 Hz, 2.49 Hz, 3.89 Hz, and 5.43 Hz, respectively. The selected frequency bandwidths are shown in Table 4. The frequency bands are divided into 0–5 Hz, 5–10 Hz, 10–15 Hz, and 15–20 Hz, respectively. The structural responses are transformed from the time domain to the frequency domain. The parameter identification is carried out in the frequency domain at the corresponding frequency bandwidth.

The comparisons of the normalized values (identified value/actual value) for system physical parameters at different frequency bands between output-input and output-only cases are displayed in Figures 5 and 6. From these figures, it can be observed that the identification performance at bandwidth I-1 and I-5 is fine for both two situations, while there are varying degrees of errors in I-2, I-3, and I-4 cases, especially at bandwidths I-3 and I-4, as the range does not cover the first five natural frequencies of the system. Under unknown excitation condition, the identification results are accurate in I-1 case but there are some errors in the identification results of the translational stiffness, the frequency, and damping ratio of TMD at high frequency bandwidth. At the same time, for input-output case, the identification results are also accurate in I-1 case

Table 3: Identification results of system physical parameters.

Excitation				Known	Unknown
Model			Theoretical	Identified	Identified
Superstructure	Damping ratio	ξ	0.02	0.02	0.02
	Stiffness	k_1 (10^8 N/m)	3.5	3.5	3.5
		k_2 (10^8 N/m)	2.5	2.5	2.5
		k_3 (10^8 N/m)	1.5	1.5	1.5
		k_4 (10^8 N/m)	1.0	1.0	1.0
		k_5 (10^8 N/m)	0.5	0.5	0.5
TMD	Frequency	f_T (Hz)	0.678	0.678	0.678
	Damping ratio	ξ_T	0.2153	0.2153	0.2153
Foundation	Stiffness	k_s (10^8 N/m)	9.54	9.54	9.54
		k_r (10^{10} N/m)	9.41	9.41	9.41
	Damping	c_s (10^7 N·s/m)	5.48	5.48	5.48
		c_r (10^9 N·s/m)	1.41	1.41	1.41

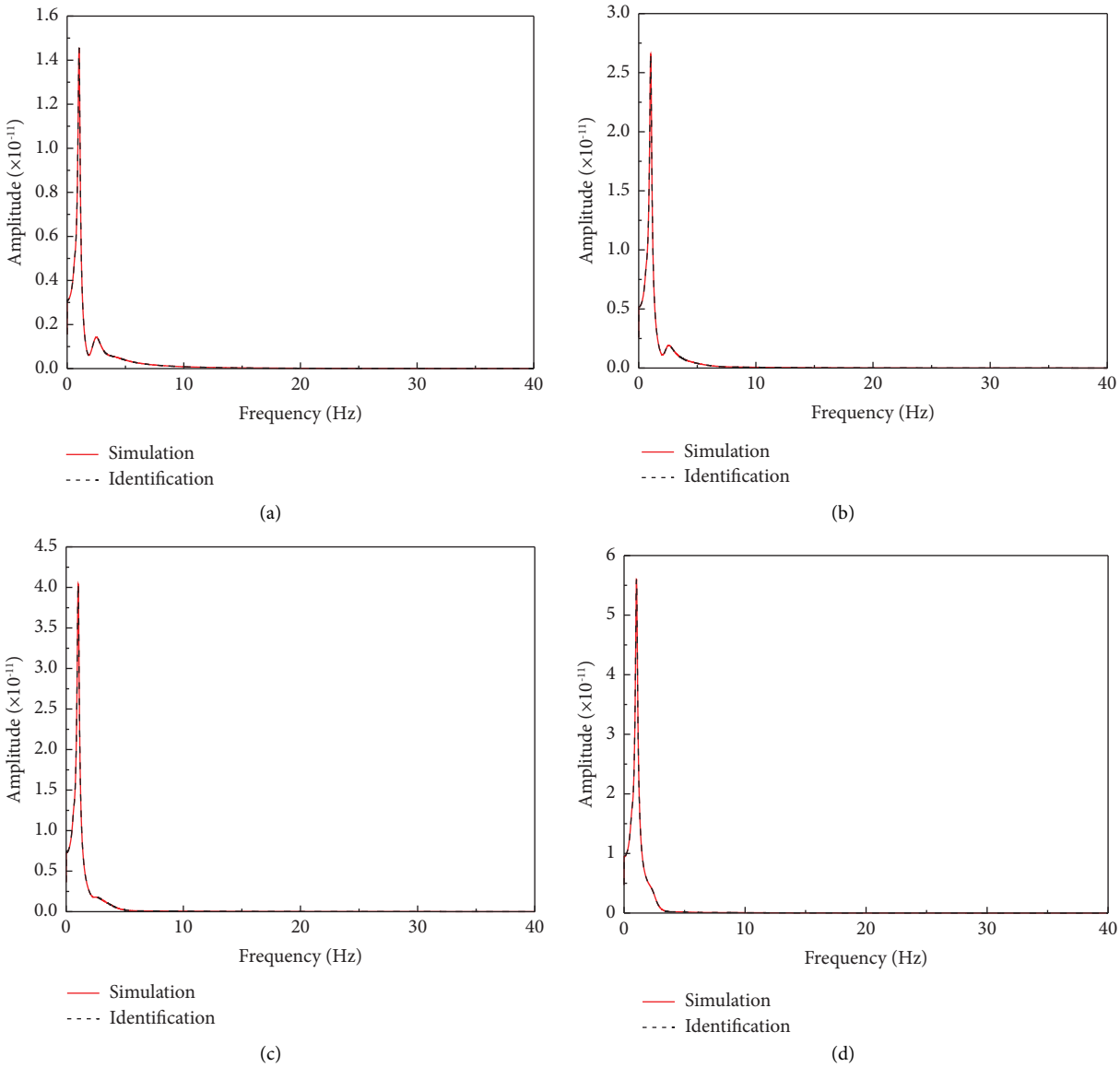

Figure 3: Continued.

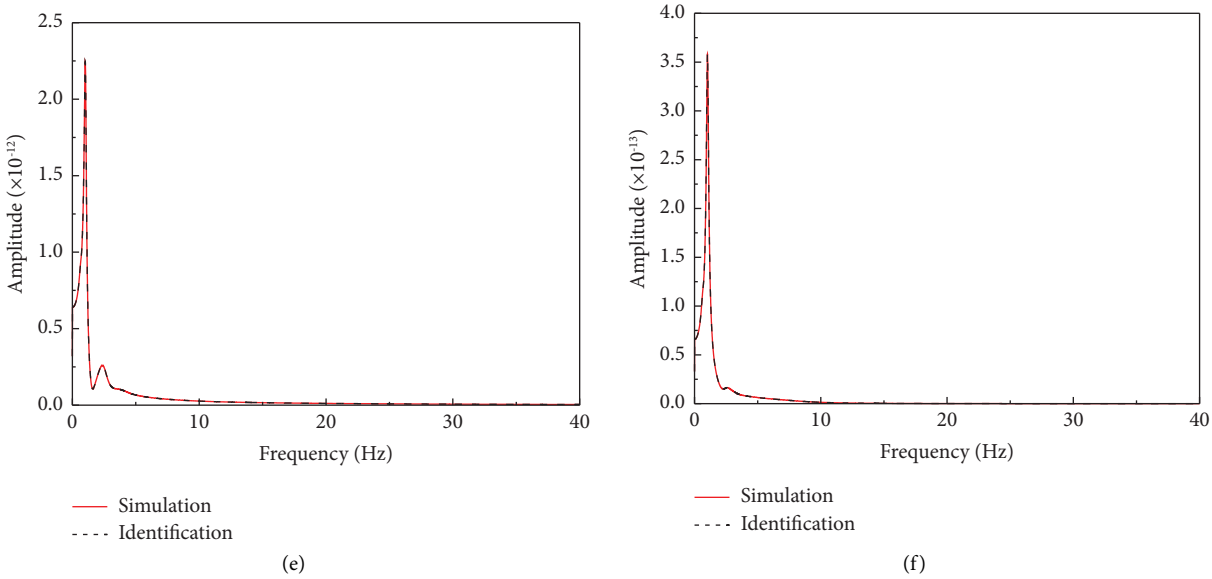

Figure 3: The frequency response function of output-input case: (a) H23; (b) H24; (c) H25; (d) H26; (e) H27; (f) H28.

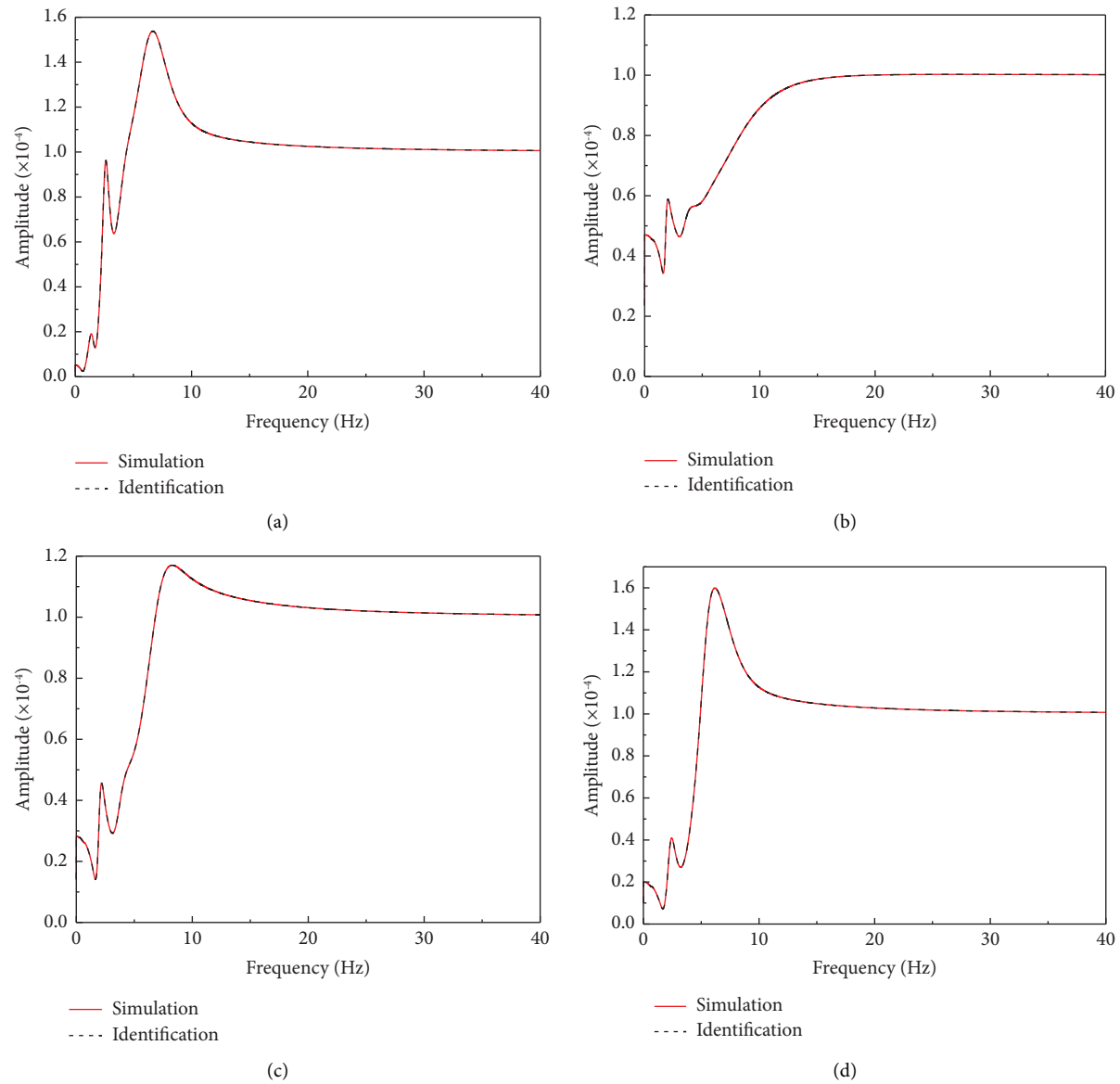

Figure 4: Continued.

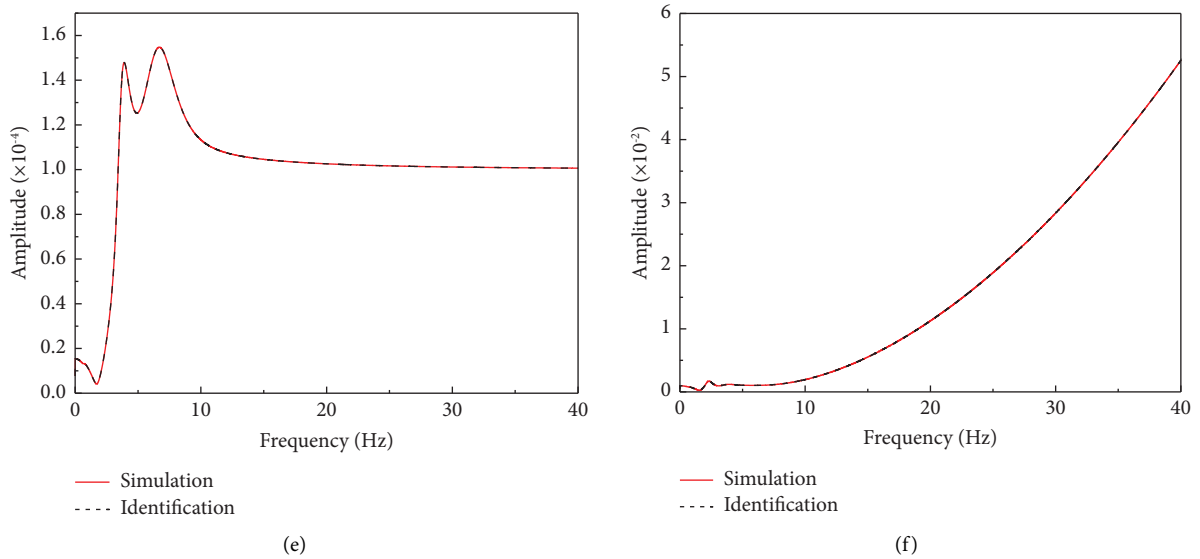

Figure 4: The transmissibility function of output-only case: (a) T12; (b) T23; (c) T24; (d) T25; (e) T26; (f) T78.

Table 4: The selected frequency bandwidth.

Case	Frequency bandwidth (Hz)
I-1	[0, 5]
I-2	[5, 10]
I-3	[10, 15]
I-4	[15, 20]
I-5	[0, 20]

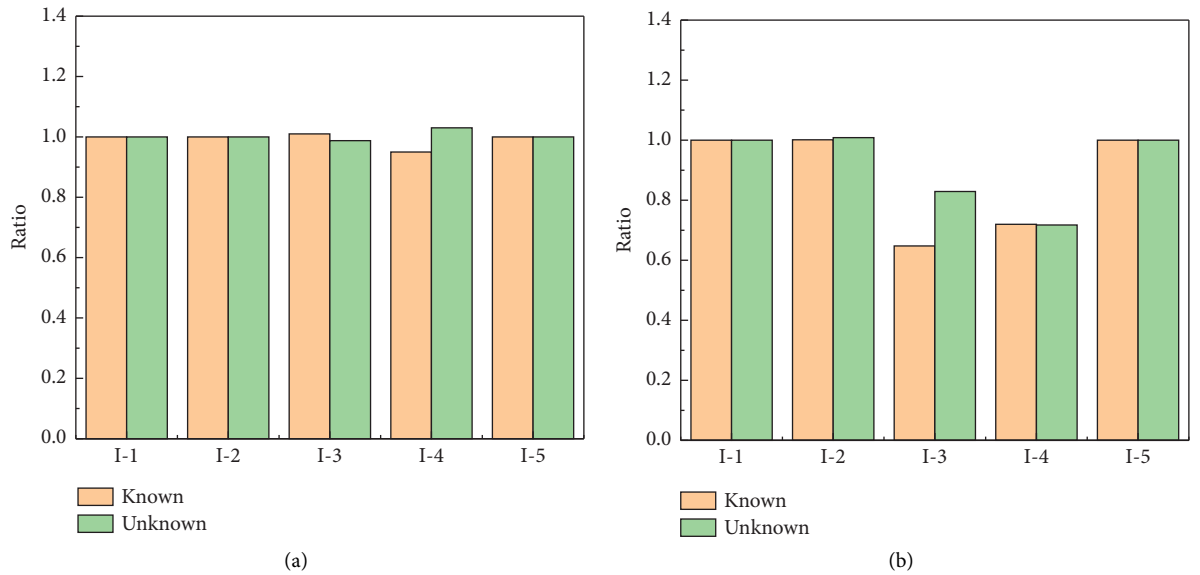

Figure 5: Continued.

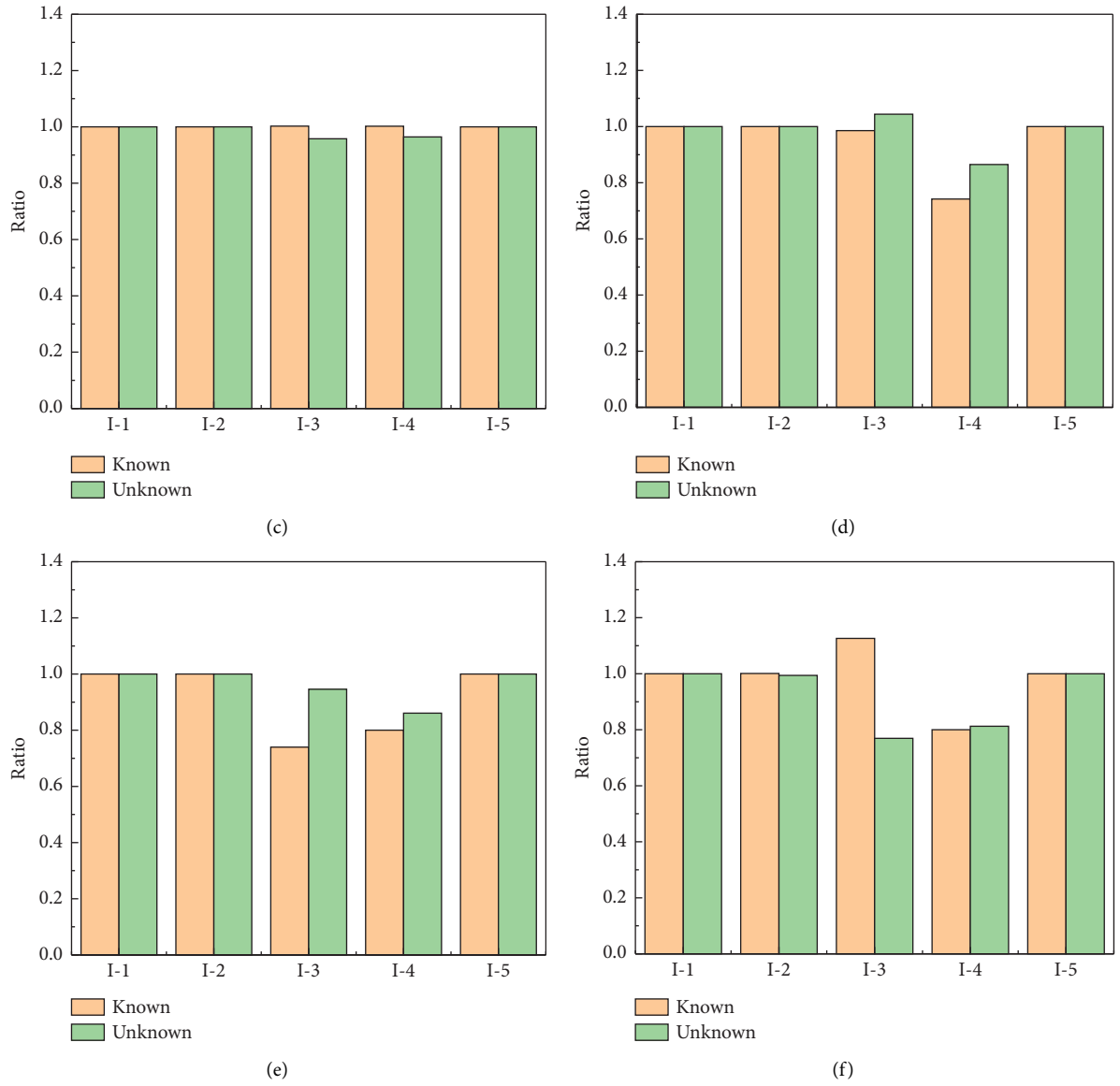

Figure 5: The normalized identification error of superstructure and TMD: (a) structure damping ratio; (b) TMD damping ratio; (c) 1st story stiffness; (d) 3rd story stiffness; (e) 5th story stiffness; (f) TMD frequency.

but some identification errors of fifth story stiffness, the frequency, and damping ratio of TMD appear at high frequency bandwidth. It is proved that using high frequency data would cause errors in the estimation results.

5.2. White Noise. The measured signals are often disturbed by noise in practical engineering. The influence of noise on the identification performance is explored in this subsection. The noise is added to the frequency function obtained from frequency domain analysis.

$$x' = x \times (1 + \varepsilon\eta), \tag{31}$$

where x and x' are the calculated value of mathematical model and the value after adding random noise; ε is the noise level; and η is a normal random variable with zero mean and unit standard deviation. The white noise cases corresponding to ε are listed in Table 5. The frequency range of 0–5 Hz is used for analyzing the noise resistance of system parameter identification.

As seen clearly from Figure 7, the normalized values of all parameters are almost equal to 1 under II-1~II-5 noise levels, indicating excellent identification performance and noise resistance. Meanwhile, it also can be found that the effects of white noise on identification accuracy of

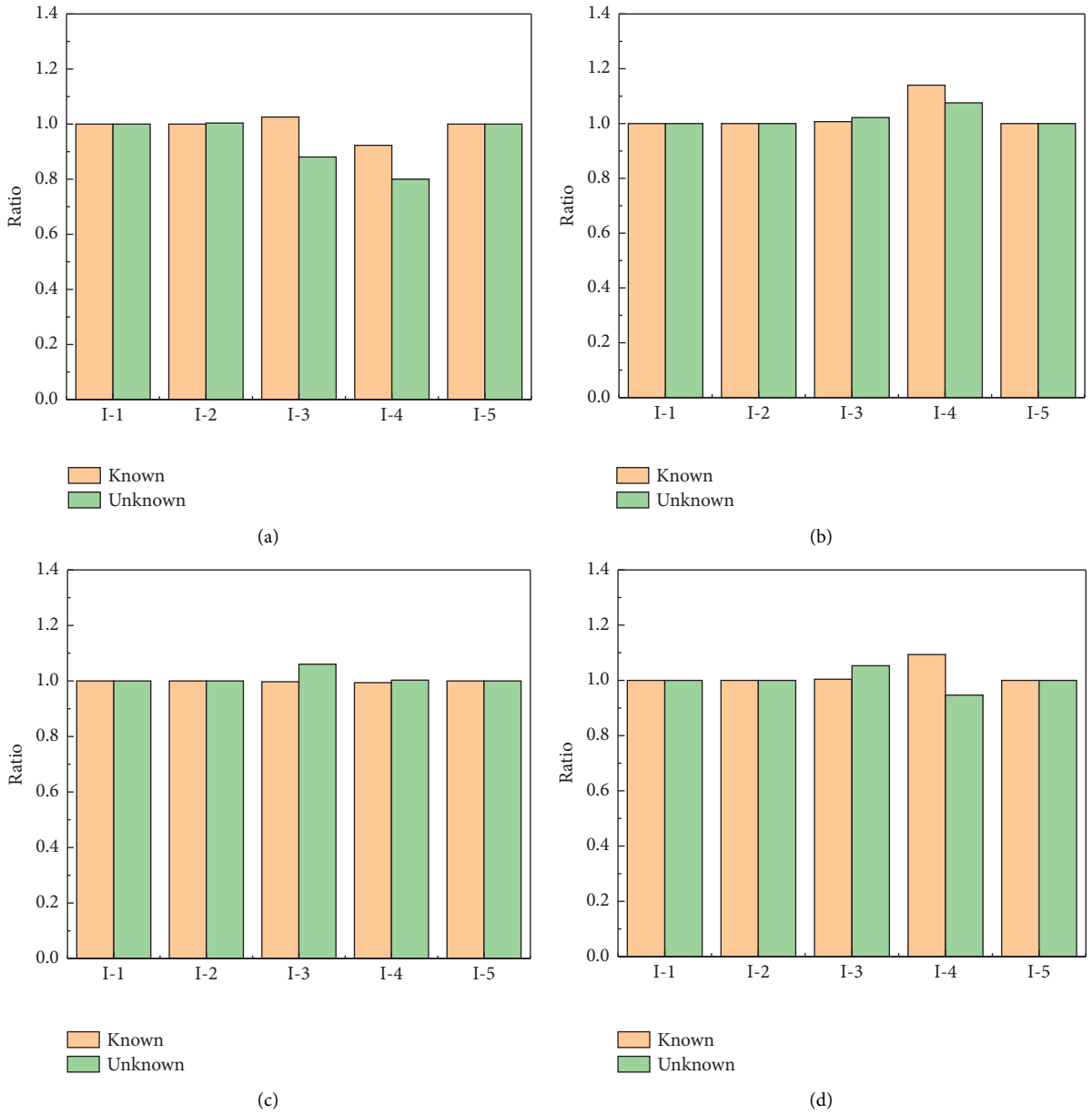

Figure 6: The normalized identification error of foundation: (a) translational stiffness; (b) rotational stiffness; (c) translational damping; (d) rotational damping.

Table 5: The white noise cases.

Case	II-1	II-2	II-3	II-4	II-5
ε	0.001	0.002	0.003	0.004	0.006

output-only case are more pronounced than those of output-input case. The identification result of foundation stiffness and damping under high noise level is not satisfactory. Hence, it ought to be emphasized that the identification accuracy of foundation parameters using measured signals for output-only case needs to be paid attention to.

5.3. Convergence. To study the convergence of APSO-SSR method and the impact of signal disturbance on parameter identification, this subsection takes three noise levels, namely, II-2, II-4, and II-5 cases, to identify physical parameters of the soil-structure-TMD system. In the identification process, the convergence criterion of this method is that the search space for structural parameters tends to stabilize. The parameter variation of II-2, II-4, and II-5 cases during the iterative process is illustrated in Figure 8. It can be seen that the parameter search space shrinks after every 50 iterations. The search space is continuously updated and reduced through the SSR strategy, gradually approaching the

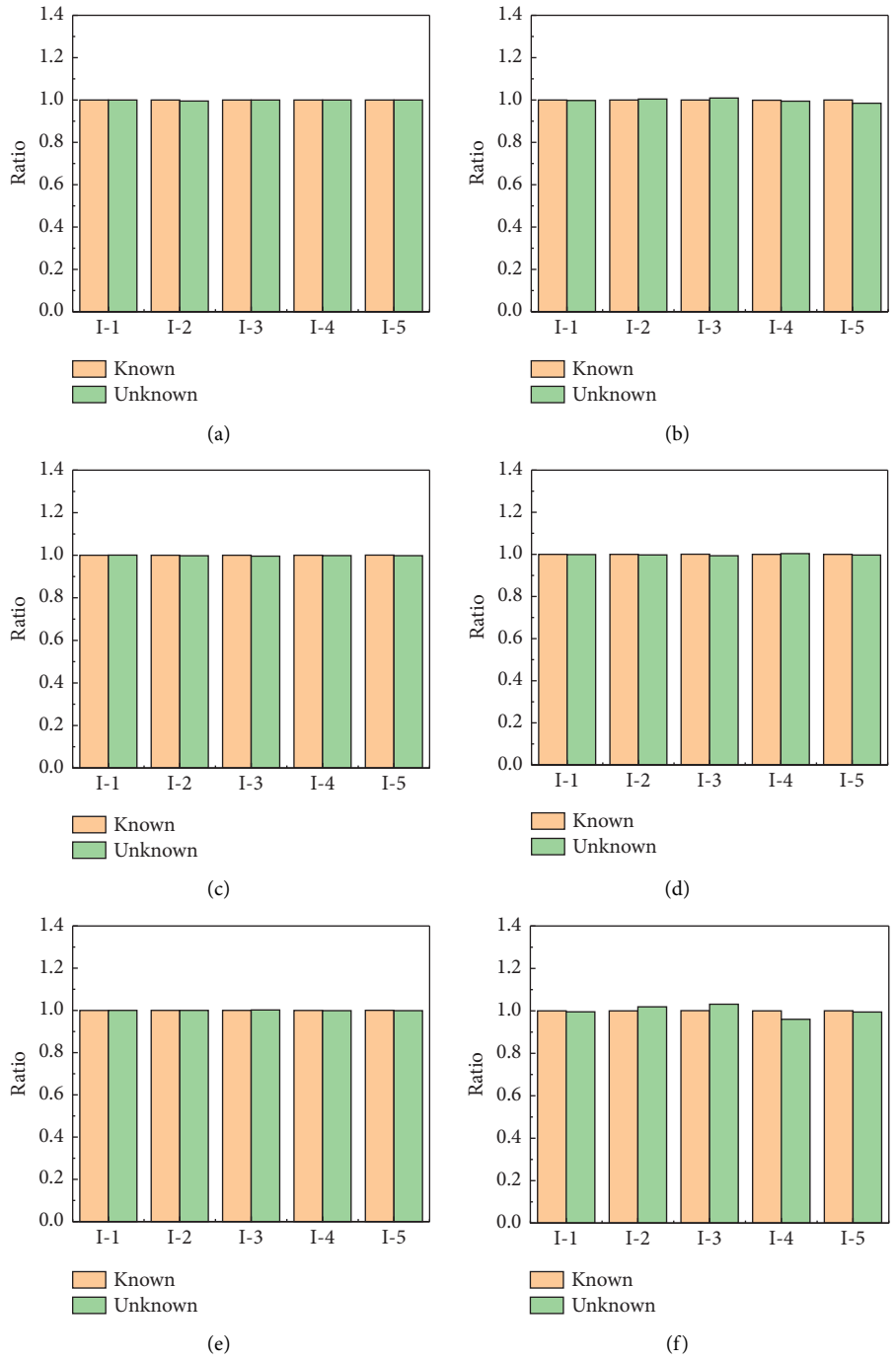

Figure 7: Continued.

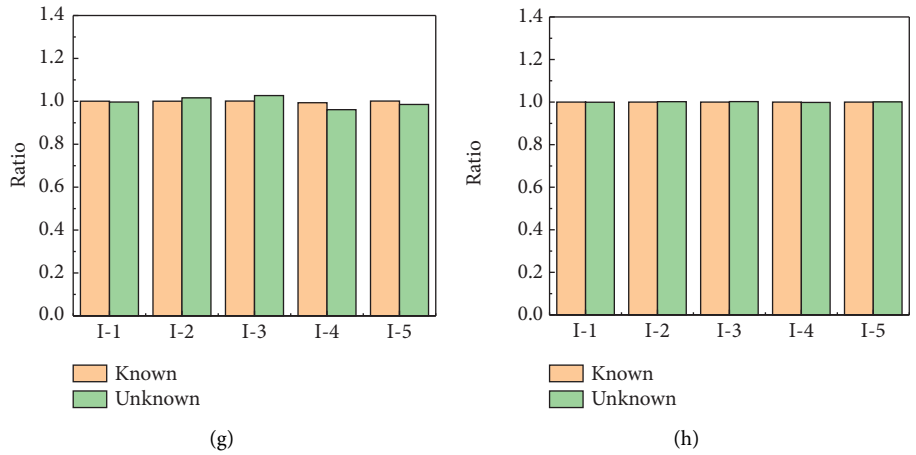

FIGURE 7: The normalized identification results after adding white noise: (a) structure damping ratio; (b) TMD damping ratio; (c) 1st story stiffness; (d) 3rd story stiffness; (e) 5th story stiffness; (f) rotational stiffness; (g) translational damping; (h) TMD frequency.

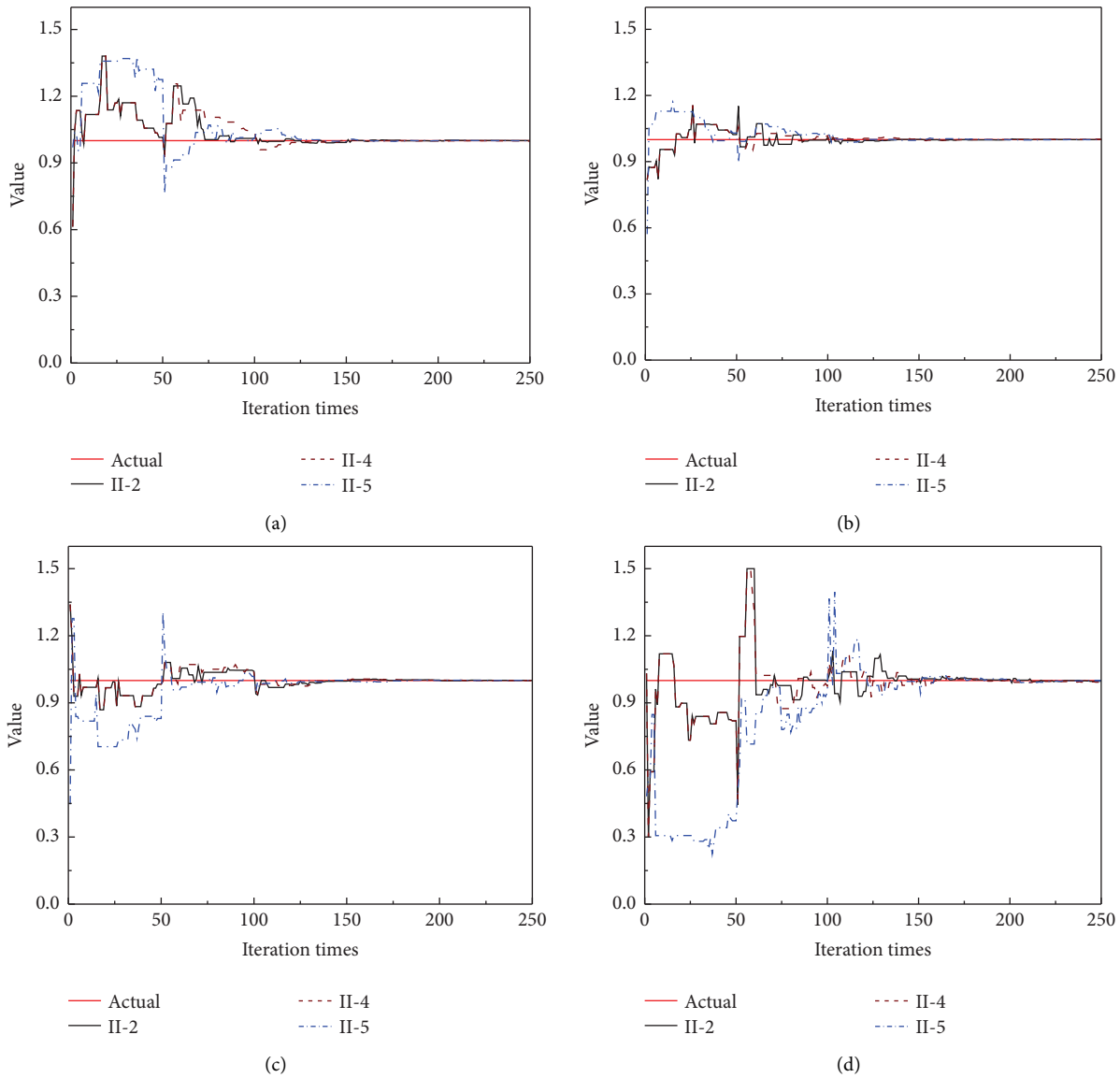

FIGURE 8: Continued.

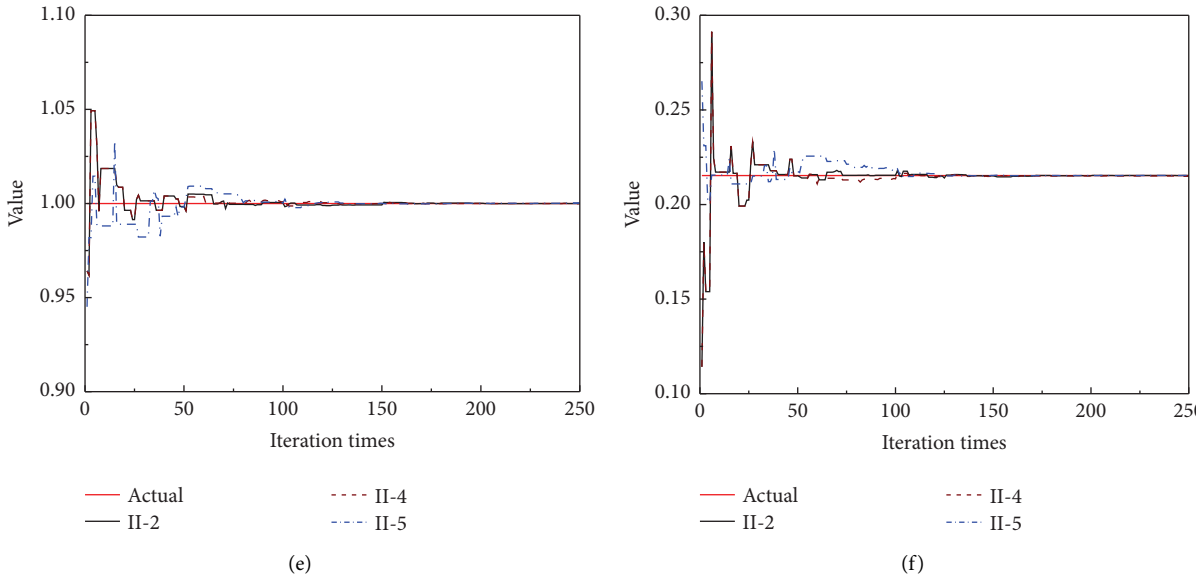

FIGURE 8: The convergence process of parameter identification under unknown excitation condition: (a) 2nd story stiffness; (b) 4th story stiffness; (c) rotational stiffness; (d) translational damping; (e) TMD frequency; (f) TMD damping ratio.

true value. The convergence results of most parameters tend to be stable after 150–200 iterations, which indicates that the parameter search domain achieves excellent convergence with small number of iterations. In addition, under different noise pollution situations, the identified parameters fluctuate greatly at the initial stage of each newly generated search space and gradually converge afterward.

6. Conclusion

This paper proposed an identification method for system physical parameters of structure equipped with TMD considering SSI effects based on the APSO-SSR method using frequency response function and transmissibility function. The physical parameter estimation framework proposed in this study is verified by numerical simulations. The following major conclusions can be made:

(1) The proposed identification method using frequency response function and transmissibility function provides reliable estimations for the system physical parameters of structure equipped with TMD considering SSI effects for output-input and input-only cases, respectively.

(2) Both for output-input and output-only cases, identification errors are prone to arise if frequency band range does not cover the first five system frequencies. Hence, the frequency band for identification should include primary frequencies of the system.

(3) The parameter identification strategies have excellent noise resistance as a whole. But white noise interference yields inaccuracy in identifying the foundation stiffness and damping, especially under unknown excitation condition.

(4) The search space reduction method effectively decreases and updates the search space during the iterative process. Although the noise pollution causes instability at the initial stage of newly generated search space, the SSR method improves the convergence speed on the premise of ensuring accuracy.

Data Availability

The data used to support the findings of this study are available from the corresponding author upon request.

Conflicts of Interest

The authors declare that they have no conflicts of interest.

Acknowledgments

This research was supported by the National Natural Science Foundation of China (grant no. 52208510). This work was also supported by Youth Program of Shandong Natural Science Foundation (grant no. ZR2022QE260). Financial support from the Postdoctoral Application Research Project of Qingdao was highly appreciated.

References

[1] L. Wang, Y. Zhou, and W. Shi, "Seismic response control of a nonlinear tall building under mainshock–aftershock sequences using semi-active tuned mass damper," *International Journal of Structural Stability and Dynamics*, vol. 23, no. 16, 2023.

[2] M. Wang, F. Sun, Y. Koetaka, L. Chen, S. Nagarajaiah, and X. Du, "Frequency independent damped outrigger systems for multi-mode seismic control of super tall buildings with frequency independent negative stiffness enhancement,"

Earthquake Engineering & Structural Dynamics, vol. 52, no. 9, pp. 2731–2754, 2023.

[3] M. Wang, F. Sun, S. Nagarajaiah, and Y. Li, "Frequency-dependency/independency analysis of damping magnification effect provided by tuned inerter absorber and negative stiffness amplifying damper considering soil-structure interaction," *Mechanical Systems and Signal Processing*, vol. 172, 2022.

[4] Z. Lu, Z. Wang, Y. Zhou, and X. Lu, "Nonlinear dissipative devices in structural vibration control: a review," *Journal of Sound and Vibration*, vol. 423, pp. 18–49, 2018.

[5] L. Wang, W. Shi, and Y. Zhou, "Adaptive-passive tuned mass damper for structural aseismic protection including soil–structure interaction," *Soil Dynamics and Earthquake Engineering*, vol. 158, 2022.

[6] F. Yang, R. Sedaghati, and E. Esmailzadeh, "Vibration suppression of structures using tuned mass damper technology: a state-of-the-art review," *Journal of Vibration and Control*, vol. 28, no. 7-8, pp. 812–836, 2022.

[7] A. Ghosh and B. Basu, "A closed-form optimal tuning criterion for TMD in damped structures," *Structural Control and Health Monitoring*, vol. 14, no. 4, pp. 681–692, 2007.

[8] M. Wang, S. Nagarajaiah, and L. Chen, "Adaptive passive negative stiffness and damping for retrofit of existing tall buildings with tuned mass damper: tmd-nsd," *Journal of Structural Engineering*, vol. 148, no. 11, 2022.

[9] M. Domizio, H. Garrido, and D. Ambrosini, "Single and multiple TMD optimization to control seismic response of nonlinear structures," *Engineering Structures*, vol. 252, 2022.

[10] S. Pan, D. Xiao, S. Xing, S. Law, P. Du, and Y. Li, "A general extended Kalman filter for simultaneous estimation of systemand unknown inputs," *Engineering Structures*, vol. 109, pp. 85–98, 2016.

[11] J. Amezquita-Sanchez, H. Park, and H. Adeli, "A novel methodology for modal parameters identification of large smart structures using MUSIC, empirical wavelet transform, and hilbert transform," *Engineering Structures*, vol. 147, pp. 148–159, 2017.

[12] C. Perez-Ramirez, J. Amezquita-Sanchez, M. Valtierra-Rodriguez, H. Adeli, A. Dominguez-Gonzalez, and R. Romero-Troncoso, "Recurrent neural network model with Bayesian training andmutual information for response prediction of large buildings," *Engineering Structures*, vol. 178, pp. 603–615, 2019.

[13] S. Ghahari, F. Abazarsa, and E. Taciroglu, "Blind modal identification of non-classically damped structures under nonstationary excitations," *Structural Control and Health Monitoring*, vol. 24, no. 6, 2017.

[14] Z. Ma, J. Choi, and H. Sohn, "Real-time structural displacement estimation by fusing asynchronous acceleration and computer vision measurements," *Computer-Aided Civil and Infrastructure Engineering*, vol. 37, no. 6, pp. 688–703, 2022.

[15] J. Love and T. Haskett, "Measuring inherent structural damping of structure-TMD systems," *Engineering Structures*, vol. 196, 2019.

[16] B. Weber and G. Feltrin, "Assessment of long-term behavior of tuned mass dampers by system identification," *Engineering Structures*, vol. 32, no. 11, pp. 3670–3682, 2010.

[17] X. Wang, Z. Zhu, and S. Au, "Bayesian operational modal analysis of structures with tuned mass damper," *Mechanical Systems and Signal Processing*, vol. 182, 2023.

[18] M. Yuan, A. Sadhu, and K. Liu, "Condition assessment of structure with tuned mass damper using empirical wavelet transform," *Journal of Vibration and Control*, vol. 24, no. 20, pp. 4850–4867, 2018.

[19] Z. Cao, X. Hua, Q. Wen, Z. Chen, and H. Niu, "A state space technique for modal identification of coupled structure-tuned mass damper systems from vibration measurement," *Advances in Structural Engineering*, vol. 22, no. 9, pp. 2048–2060, 2019.

[20] B. Cho, J. Jo, S. Joo, and H. Kim, "Dynamic parameter identification of secondary mass dampers based on full-scale tests," *Computer-Aided Civil and Infrastructure Engineering*, vol. 27, no. 3, pp. 218–230, 2012.

[21] A. Roffel and S. Narasimhan, "Extended Kalman filter for modal identification of structures equipped with a pendulum tuned mass damper," *Journal of Sound and Vibration*, vol. 333, no. 23, pp. 6038–6056, 2014.

[22] S. Schleiter and O. Altay, "Identification and semi-active control of structures with abrupt stiffness degradations," *Mechanical Systems and Signal Processing*, vol. 163, 2022.

[23] J. Hwang, D. Kwon, and A. Kareem, "A modal-based Kalman filtering framework for mode extraction and decomposition of damped structures," *Computer-Aided Civil and Infrastructure Engineering*, vol. 38, no. 10, pp. 1274–1289, 2022.

[24] D. Pan, J. Tan, X. Fu, Y. Huang, and X. Li, "Modal analysis and extraction method for the frame structure considering soil-structure interaction effect," *Computers and Geotechnics*, vol. 157, 2023.

[25] B. Bapir, L. Abrahamczyk, T. Wichtmann, and L. Prada-Sarmiento, "Soil-structure interaction: a state-of-the-art review of modeling techniques and studies on seismic response of building structures," *Frontiers in Built Environment*, vol. 9, 2023.

[26] S. Liu, Z. Lu, P. Li, S. Ding, and F. Wan, "Shaking table test and numerical simulation of eddy-current tuned mass damper for structural seismic control considering soil-structure interaction," *Engineering Structures*, vol. 212, 2020.

[27] S. Liu, Z. Lu, P. Li, W. Zhang, and E. Taciroglu, "Effectiveness of particle tuned mass damper devices for pile-supported multi-story frames under seismic excitations," *Structural Control and Health Monitoring*, vol. 27, no. 11, 2020.

[28] R. Jabary and S. Madabhushi, "Tuned mass damper effects on the response of multi-storied structures observed in geotechnical centrifuge tests," *Soil Dynamics and Earthquake Engineering*, vol. 77, pp. 373–380, 2015.

[29] R. Jabary and G. Madabhushi, "Tuned mass damper positioning effects on the seismic response of a soil-MDOF-structure system," *Journal of Earthquake Engineering*, vol. 22, no. 2, pp. 281–302, 2018.

[30] F. Jia and L. Jianwen, "Performance degradation of tuned-mass-dampers arising from ignoring soil- structure interaction effects," *Soil Dynamics and Earthquake Engineering*, vol. 125, 2019.

[31] A. Abd-Elhamed and S. Mahmoud, "Simulation analysis of TMD controlled building subjected to far- and near-fault records considering soil-structure interaction," *Journal of Building Engineering*, vol. 26, 2019.

[32] D. Gorini and C. Chisari, "Impact of soil-structure interaction on the effectiveness of tuned mass dampers," *Earthquake Engineering & Structural Dynamics*, vol. 51, no. 6, pp. 1501–1521, 2022.

[33] F. Khoshnoudian, R. Ziaei, P. Ayyobi, and F. Paytam, "Effects of nonlinear soil-structure interaction on the seismic response of structure-TMD systems subjected to near-field earthquakes," *Bulletin of Earthquake Engineering*, vol. 15, no. 1, pp. 199–226, 2017.

[34] W. Zhang, S. Liu, M. Shokrabadi, A. Dehghanpoor, and E. Taciroglu, "Nonlinear seismic fragility assessment of tall buildings equipped with tuned mass damper (TMD) and considering soil-structure interaction effects," *Bulletin of Earthquake Engineering*, vol. 20, no. 7, pp. 3469–3483, 2022.

[35] G. Espinoza, E. Casanova, F. Benedetti, R. Mena, and J. Almazán, "Optimal TMD design for torsional balance of asymmetrical 3D structures considering soil-structure interaction," *Structural Control and Health Monitoring*, vol. 29, no. 1, 2022.

[36] G. Bekdaş and S. Nigdeli, "Metaheuristic based optimization of tuned mass dampers under earthquake excitation by considering soil-structure interaction," *Soil Dynamics and Earthquake Engineering*, vol. 92, pp. 443–461, 2017.

[37] N. Djedoui and A. Ounis, "Optimization of TMD parameters in frequency domain including SSI effect by means of recent metaheuristic algorithms," *Practice Periodical on Structural Design and Construction*, vol. 27, no. 3, 2022.

[38] Z. Gao, M. Zhao, Y. Wu, M. Wang, and X. Du, "Parameter design and performance evaluation of tuned mass damper (TMD) for seismic control of structure considering soil-structure interaction (SSI)," *Structures*, vol. 52, pp. 1116–1129, 2023.

[39] C. Devriendt and P. Guillaume, "Identification of modal parameters from transmissibility measurements," *Journal of Sound and Vibration*, vol. 314, no. 1-2, pp. 343–356, 2008.

[40] C. Devriendt, G. De Sitter, and P. Guillaume, "An operational modal analysis approach based on parametrically identified multivariable transmissibilities," *Mechanical Systems and Signal Processing*, vol. 24, no. 5, pp. 1250–1259, 2010.

[41] S. Hassan, R. Ibrahim, N. Saad, V. Asirvadam, and K. Bingi, "Hybrid APSO-spiral dynamic algorithms with application to tuning of filtered PPI controller in a wirelessHART Environment," *Journal of Intelligent and Fuzzy Systems*, vol. 37, no. 1, pp. 597–610, 2019.

[42] S. Talatahari, E. Khalili, and S. Alavizadeh, "Accelerated particle swarm for optimum design of frame structures," *Mathematical Problems in Engineering*, vol. 3, 2013.

[43] J. Agrawal and S. Agrawal, "Acceleration based particle swarm optimization (APSO) for RNA secondary structure prediction," *Progress in Systems Engineering*, vol. 1089, pp. 741–746, 2015.

[44] A. Charalampakis and V. Koumousis, "Identification of Bouc-Wen hysteretic systems by a hybrid evolutionary algorithm," *Journal of Sound and Vibration*, vol. 314, no. 3-5, pp. 571–585, 2008.

[45] H. Sun and R. Betti, "Simultaneous identification of structural parameters and dynamic input with incomplete output-only measurements," *Structural Control and Health Monitoring*, vol. 21, no. 6, pp. 868–889, 2014.

[46] N. Gong, P. Li, J. Shan, and Y. Ouyang, "Data-driven identification and modeling of earthquake-excited building structures regarding soil-structure interaction," *The Structural Design of Tall and Special Buildings*, vol. 29, no. 18, 2020.

[47] Z. Pap and L. Kollár, "The dynamic response of infinitely long constrained bars and its application for modelling SSI," *Structures*, vol. 34, pp. 875–885, 2021.

[48] S. Ghahari, F. Abazarsa, M. Ghannad, and E. Taciroglu, "Response-only modal identification of structures using strong motion data," *Earthquake Engineering & Structural Dynamics*, vol. 42, no. 8, pp. 1221–1242, 2013.

[49] F. Sadek, B. Mohraz, A. Taylor, and R. Chung, "A method of estimating the parameters of tuned mass dampers for seismic application," *Earthquake Engineering & Structural Dynamics*, vol. 26, no. 6, pp. 617–635, 1997.

[50] J. Salvi, F. Pioldi, and E. Rizzi, "Optimum tuned mass dampers under seismic soil-structure interaction," *Soil Dynamics and Earthquake Engineering*, vol. 114, pp. 576–597, 2018.

[51] T. Datta, *Seismic Analysis of Structures*, Wiley, New York, NY, USA, 2010.

[52] S. Liu, H. Li, J. Xie, S. Yang, and P. Li, "Comparative study on seismic performance of structure with TMD and particle TMD considering SSI effects," *Journal of Building Engineering*, vol. 77, 2023.

[53] T. Heiland, H. Aji, F. Wuttke, L. Stempniewski, and A. Stark, "Influence of soil-structure interaction on the dynamic characteristics of railroad frame bridges," *Soil Dynamics and Earthquake Engineering*, vol. 167, 2023.

[54] W. Li and Q. Chen, "Effect of vertical ground motions and overburden depth on the seismic responses of large underground structures," *Engineering Structures*, vol. 205, 2020.

[55] D. Pitilakis and D. Clouteau, "Equivalent linear substructure approximation of soil-foundation-structure interaction: model presentation and validation," *Bulletin of Earthquake Engineering*, vol. 8, no. 2, pp. 257–282, 2010.

[56] D. Forcellini, "A 3-DOF system for preliminary assessments of the interaction between base isolation (BI) technique and soil structure interaction (SSI) effects for low-rise buildings," *Structures*, vol. 59, 2024.